Nano Research 2015, 8(7): 2216–2222
DOI 10.1007/s12274-015-0731-0
Research Article
ISSN 1998-0124
CN 11-5974/O4

Germanium nanopyramid arrays showing near-100% absorption in the visible regime

Qi Han[1], Yongqi Fu[1] (✉), Lei Jin[1], Jingjing Zhao[2], Zongwei Xu[3], Fengzhou Fang[3], Jingsong Gao[2], and Weixing Yu[4]

[1] *School of Physical Electronics, University of Electronic Science and Technology of China, Chengdu 610054, China*
[2] *Changchun Institute of Optics, Fine Mechanics and Physics, Chinese Academy of Sciences, Changchun 130033, China*
[3] *Key Laboratory of Precision Measuring Technology & Instruments, Centre of Micro-Nano Manufacturing Technology, Tianjin University, Tianjin 300072, China*
[4] *Institute of Micro & Nano Optics, College of Optoelectronic Engineering, Shenzhen University, Shenzhen 518060, China*

Received: 10 November 2014
Revised: 14 January 2015
Accepted: 16 January 2015

KEYWORDS
nanopyramid array, absorption coefficient, antireflection coatings, slow-light mode

ABSTRACT

Solar energy is regarded as one of the most plentiful sources of renewable energy. An extraordinary light-harvesting property of a germanium periodic nanopyramid array is reported in this Letter. Both our theoretical and experimental results demonstrate that the nanopyramid array can achieve perfect broadband absorption from 500- to 800-nm wavelength. Especially in the visible regime, the experimentally measured absorption can even reach 100%. Further analyses reveal that the intrinsic antireflection effect and slow-light waveguide mode play an important role in the ultra-high absorption, which is helpful for the research and development of photovoltaic devices.

1 Introduction

Development of sustainable energy has been a challenging problem for human beings in the current century. Recently, tremendous progress has been made in the development of photovoltaics that can potentially be mass deployed because photovoltaic cells can serve as a virtually unlimited, clean source of energy by converting sunlight into electrical power [1–4]. During this progress, the enhancement of optical absorption has been focused upon as an effective and powerful method to boost energy-conversion efficiencies. The ability to harvest sunlight is of profound interest for high-performance solar-cell applications. Conventional silicon thin-film-based photovoltaic cells are inefficient, although nanostructures in silicon photovoltaic cells are of particular importance, as they currently constitute over 80% of the worldwide photovoltaic market [5]. Silicon-based photovoltaic cells have a short collection length for excited carriers, resulting in a significant

Address correspondence to yqfu@uestc.edu.cn

improvement in carrier collection efficiency. However, silicon absorbs poorly over the peak of the solar spectrum, necessitating the use of Si wafers of thickness greater than 100 μm for sufficient absorption. Germanium is an indirect-band-gap material, as is silicon. However, germanium has a lower band gap, enabling photons with lower energy to excite electrons, which migrate from the valence band to the conduction band. Accordingly, electron–hole pairs are produced. This implies that germanium thin-film-based structures would have increased optical absorption coefficient in a broader band compared to that of silicon thin-film-based structures. Furthermore, for germanium structures, in comparison with silicon structures, more heat can be produced with the same photon-excitation energy; higher temperatures improve the efficiency of generation and separation of electron–hole pairs as well as photoelectric conversion efficiency. In other words, germanium-based structures have higher internal quantum efficiency and short-circuit current; consequently, germanium-based photovoltaic cells have higher efficiency.

Although thin-film photovoltaic cells offer a viable pathway to reduce fabrication costs and material usage [6], their energy-conversion efficiencies can still be improved significantly by enabling them to harness a larger fraction of incident solar photons. In this regard, simulation studies have previously shown that three-dimensional (3D) cell structures such as nanowire arrays [7–10], nanopillar arrays [11–13], nanocone arrays [14–16], nanohole arrays [17–20], nanodisk arrays [21, 22], and other perfect absorbers [23–26] possess unique optical characteristics for absorbing and harvesting light. Germanium nanopyramid arrays can improve the absorption coefficient because of an intrinsic antireflection effect [15] and stimulating the slow-light waveguide mode of weakly coupled resonances [10, 27]. In this Letter, both theoretical and experimental investigations are performed to show that the germanium nanopyramid arrays have the ability to reach perfect absorption in the visible regime.

2 Experimental

A germanium thin film of 1-μm thickness supported by a silica glass substrate was coated using the electron-beam evaporation technique. Figure 1(a) shows a schematic illustration of the periodic nanopyramid structure. The nanofabrication experiment was performed using our focused ion beam (FIB) machine (FEI NOVA200, Nanolab) equipped with a liquid-gallium ion source. The FIB machine is integrated with

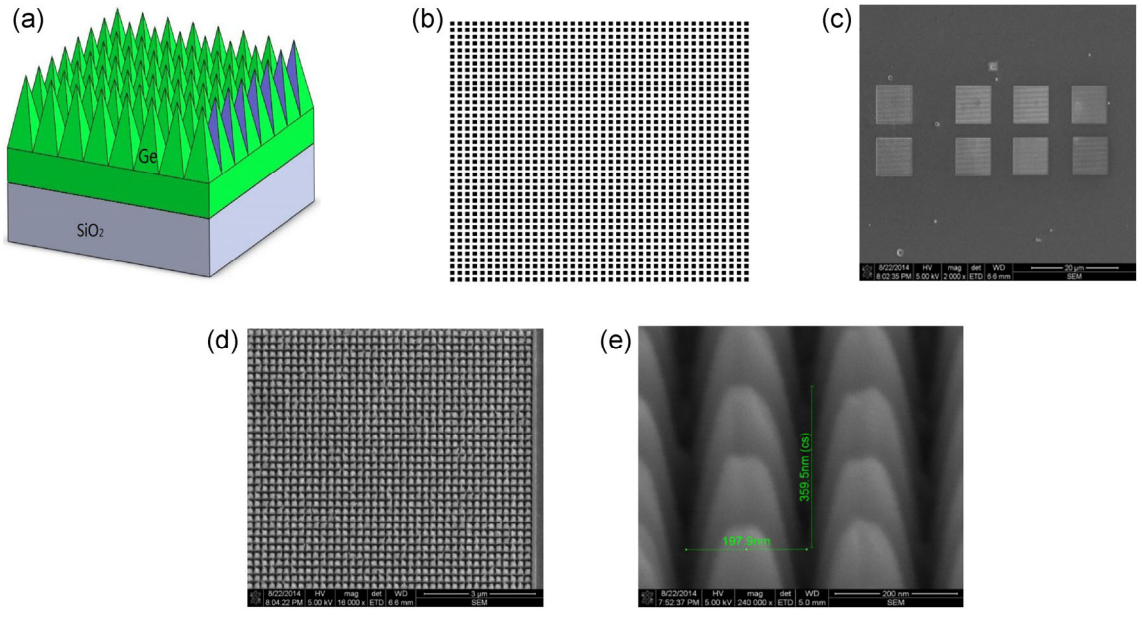

Figure 1 (a) Schematic diagram of the nanopyramid-array absorber; (b) binary bitmap pattern designed for fabricating the nanopyramid array; (c) overall SEM images of eight nanopyramid arrays; (d) SEM image of a germanium nanopyramid array; (e) zoomed-in SEM images of the germanium nanopyramid arrays with measured sizes in the vertical and horizontal directions.

scanning electron microscope (SEM) and gas-assisted etching (GAE) functions. Further, the FIB machine employs focused Ga^+ ion-beam milling at 30 keV, a probe current of 4 pA–19.7 nA, and a beam-limiting aperture size of 25–350 μm. For the smallest beam currents, the beam was focused to 5 nm in diameter at full width and half maximum (FWHM). Assisted by a computer program, the milling process is performed by varying the ion dose for different relief depths. The defined area for FIB milling using a bitmap function [28, 29] is 9 μm × 9 μm. In the milling process, a beam current and ion dose of 20 pA and 0.25 nC/μm^2, respectively, were adopted. The working distance from the sample surface to the ion-column facet was 20 mm. The electron mode of FIB milling was selected for the germanium thin film. The charging effect originating from germanium was low during scanning and could be ignored. Unlike the milling of conventional two-dimensional (2D) structures, one-step FIB milling of 3D patterns is quite challenging. Firstly, precise calibration is required to ensure accurate milling depth. Then, a designed 2D pattern (see Fig. 1(b)) was introduced into the defined milling area. The feature size of the pattern was defined on the basis of the rate of the self-extension effect generated by the redeposition effect of ion-beam bombardment while designing the pattern. Initially, a concave V-shaped reverse pyramid structure a few nanometers in depth was produced. After continuous milling for 15 min, the square areas are over-milled to enable the reverse pyramid structure originating from the square area to extend and are joined each other between the two adjacent square areas, thereby forming the 3D pyramid array.

3 Results and discussion

Figures 1(c), 1(d), and 1(e) show SEM images of the nanopyramid arrays. For convenient characterization, a total of eight nanopyramid arrays were fabricated on the germanium thin film, and the side length of each square nanopyramid array was determined to be 20 μm. These germanium nanopyramid arrays had a uniform height of approximately 500 nm and bottom length of approximately 200 nm. All germanium nanopyramid arrays are closely packed and display short-range ordering.

For designing nanopyramid structures, wave effects must be considered by solving Maxwell's equations for the full wave vector. A finite-difference time-domain (FDTD) algorithm has been proven effective for numerically simulating such periodic structures. In our analyses, we use FDTD solution 8.5 (Lumerical Solution Inc.) and set a fine grid of dimensions 5 nm × 5 nm × 5 nm, which is less than 1/100 of the shortest wavelength in the entire computational domain, to ensure convergence in the calculation process. The wavelength ranges from 500 to 800 nm. Figure 2(a) shows the experimental setup for spectroscopy.

The absorption spectra of the nanopyramid arrays and thin film are shown in Figs. 2(b) and 2(c), respectively. In order to obtain a realistic simulation, we placed eight nanopyramid arrays in the field of view. The absorption spectrum is the average of those of eight nanopyramid arrays. We observed a substantial enhancement in absorption over the entire usable solar spectrum in the nanopyramid array structure. In comparison to the experimental results, the corresponding numerical calculation results show that the absorption coefficient decreases slightly from 1 to 0.983 in the nanopyramid arrays, but the absorption coefficient remains at the level of perfect absorption, which is higher than those in previous reports [10, 15, 24, 27]. The absorption coefficient is higher than those of other reported nanostructures in the wavelength range from 400 to 800 nm. Absorption coefficient in the calculation is lower than that obtained in experiments. This can be attributed to SiO_2 impurities in the sample, which play a dominant role in increasing the absorption coefficient as an antireflection coating. The ultra-high absorption may be explained in detail from a physical perspective as follows.

Considering the high refractive-index contrast between germanium and air, a large portion of incident light is reflected from the surface of the germanium thin film and thus cannot be used to generate current in future solar cells. Currently, quarter-wavelength transparent thin films are the industrial standard for antireflection coatings in thin-film solar cells. However, these quarter-wavelength antireflection coatings are typically designed to suppress reflection at a specific wavelength [30, 31]. In the nanopyramid arrays, the electromagnetic field can be coupled efficiently into the cavity of the pyramids at resonance, resulting in a significant boost in light-trapping ability. For

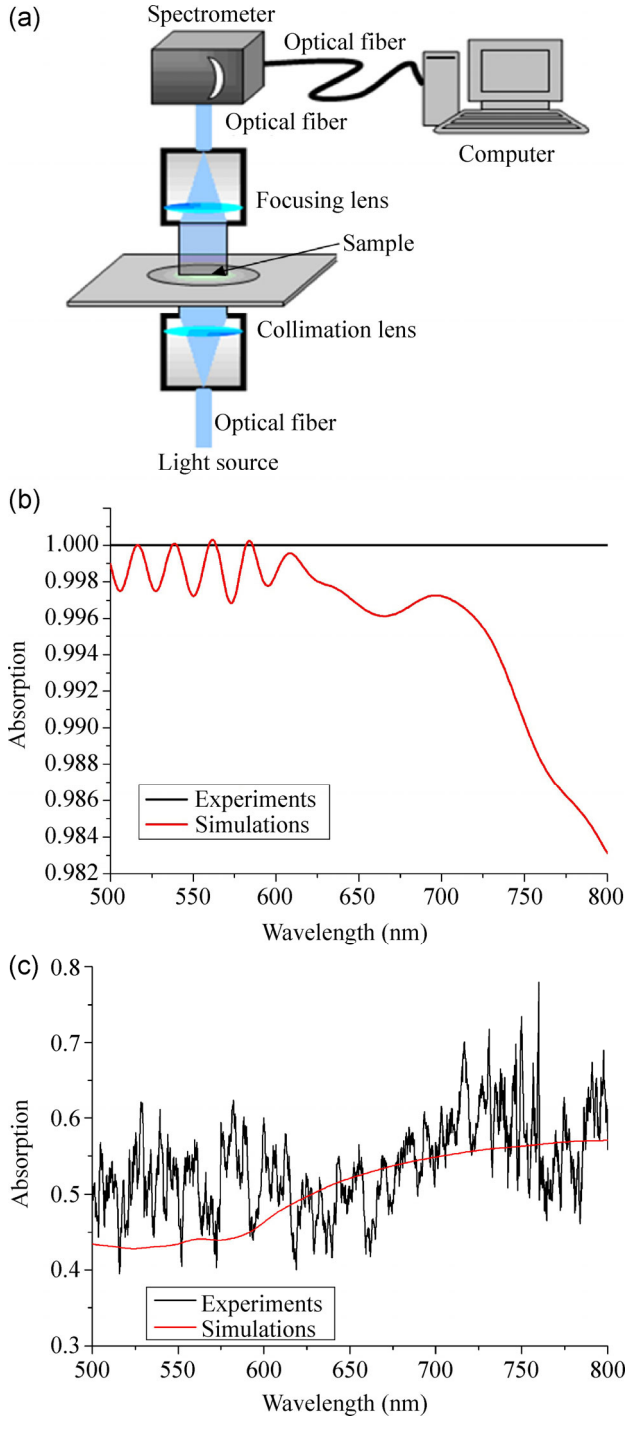

Figure 2 (a) Experimental setup of the spectrometry system: An optical fiber-based spectrometer from Ocean Optics is employed. (b) Measured and simulated results of absorption coefficient of samples with nanopyramid arrays. (c) Measured and simulated results of absorption coefficient of samples with a flat thin film.

nanopyramid arrays with a low fill factor, most of the incident light cannot be coupled into the nanopyramid arrays; instead, it is absorbed in a single path through the array. In contrast, nanopyramid arrays with a high fill factor provide efficient supporting modes. Hence, the absorption is greatly increased when these modes are well coupled and concentrated in the array [32].

The contribution to light-absorption enhancement from the structured area, as shown in Fig. 2(b), originates from lighting trapping and the antireflection effect, in contrast to the absorption in the flat thin film without any structures shown in Fig. 2(c). The nanopyramid arrays suppress reflection because the pyramid geometry provides an averaged, graded index from air to germanium as the side length increases from zero to the maximum value at the planar film surface. The reflection suppression is broadband because the index matching is largely independent of wavelength. On the other hand, the nanostructures can be regarded as a special type of metamaterial. To achieve effective antireflection, the array periodicity is in the subwavelength regime based on the incoming light to observe an effective averaged index [15]. In addition, arrays with a high aspect ratio are preferred for obtaining a smooth index transition from air to germanium.

Meanwhile, ultra-short vertical waveguides based on nanopyramid arrays support the slow-light mode at different wavelengths so that the incident light at different wavelengths is captured at the position of different tooth widths (lateral size of the single pyramid). As can be seen in Fig. 3, light is mainly absorbed on the top or edge of nanopyramid. Most of the incident energy first propagates downward along the *z*-direction in the air-gap region without penetrating the nanopyramid arrays and then whirls into the nanopyramid region. The whirling forms vortexes close to the interface between the nanopyramid and air regions. The vortexes are located at the positions where the electromagnetic field is highly concentrated. These are typical features in slow-light waveguides with the slow light defined as the propagation of light at a group velocity that is quite low in comparison to the speed of light in vacuum [33–35]. For example, in Ref. [33], the authors demonstrated that a designed air/dielectric/metal waveguide could support a vortex mode propagating very slowly along the slab and even becoming trapped at a critical core thickness. Later, a

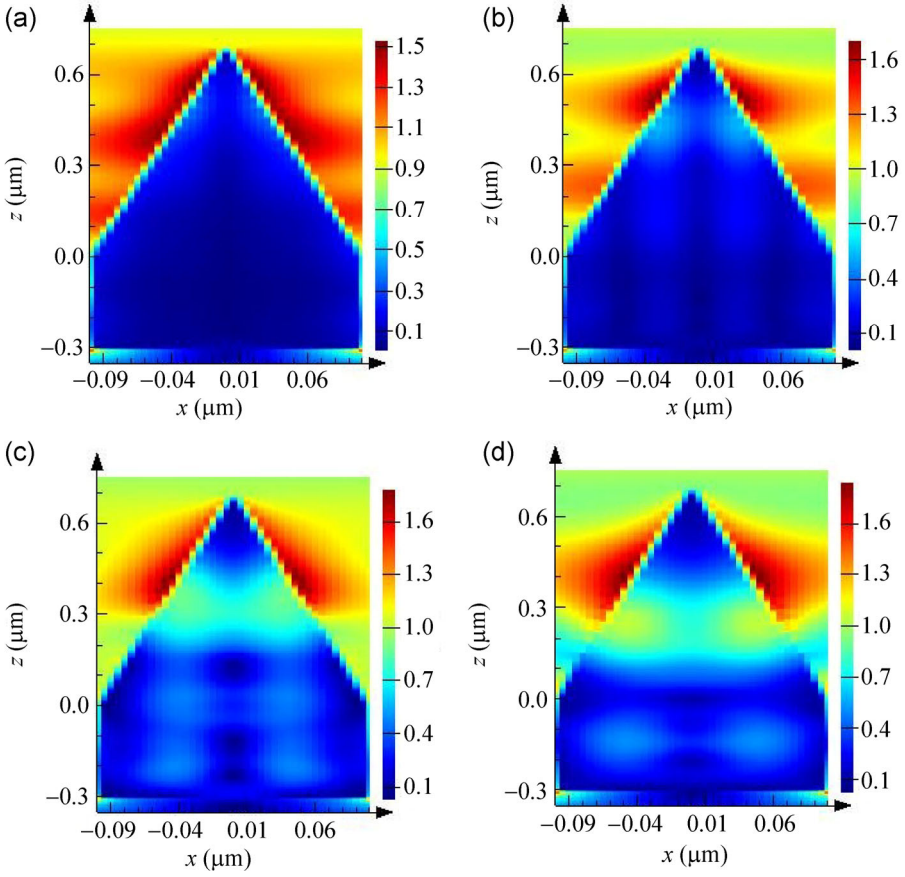

Figure 3 Electromagnetic field distribution at the $y = 0$ plane for different wavelengths: (a) $\lambda = 500$ nm, (b) $\lambda = 600$ nm, (c) $\lambda = 700$ nm, and (d) $\lambda = 800$ nm.

nanopyramid/air/nanopyramid slow-light waveguide was demonstrated to slow down propagating electromagnetic waves to a complete standstill at certain regions of the air-core waveguide. Light with different wavelengths or different photon energies exhibit different penetration depths. Most of short-wavelength light is absorbed on nanopyramid arrays. On increasing the wavelength, the focusing regime of the electromagnetic field is shifted to the bottom of the nanopyramid, implying that light with different wavelengths is absorbed in the nanopyramid arrays.

In order to intuitively observe the absorption effect on the structured and non-structured areas, we utilized an apertured near-field scanning optical microscope (a-NSOM; Multiview 2000^{TS}, Nanonics Inc.) to obtain the optical-intensity distributions. First, we selected the working mode of confocal imaging in which the sample is stationary and only the stage is scanned in horizontal plane. This is finely focused far-field imaging with resolution within the diffraction limit. The fiber tip is not necessary in this imaging mode. Intensity distributions can be derived from the confocal images, as shown in Fig. 4. As can be seen from Figs. 4(a) and 4(b), the optical intensity in the nanopyramid arrays and flat thin film are distinct; nevertheless, the imaging resolution is low compared to the feature size of the structures. It can be seen from the color bar that the intensity in the nanopyramid arrays is approximately zero, and in the flat thin film, the intensity is approximately 0.06 with a maximum intensity of 0.16. This result is consistent with the absorption coefficient discussed above. Figure 4(c) shows the intensity distribution in a section of the sample involving both structured and non-structured areas for comparison. It can be seen that the intensity in the nanopyramid arrays and flat thin film are different with color-scale variation from 0 to 0.20. Similarly, Fig. 4(d) shows the corresponding near-field image of the hybrid section. A flat-thin-film portion adjacent to nanopyramid arrays in the hybrid section can partially absorb light

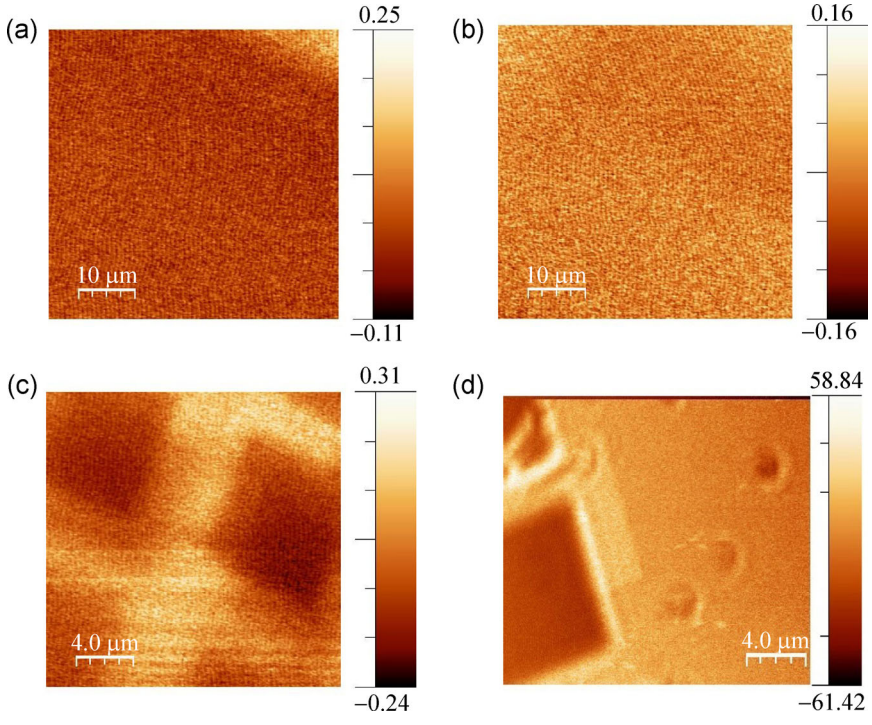

Figure 4 Intensity distributions for both structured and non-structured areas: (a) nanopyramid arrays with a scan area of 5 μm × 5 μm, (b) flat thin film with a scan area of 5 μm × 5 μm, and (c) hybrid section (bright part indicates the flat thin film) with a scan area of 20 μm × 20 μm. (d) NSOM image of the hybrid section. The color bars indicate the relative light intensity. The value approaching 0 indicates near-100% absorption from the area with nanopyramid arrays.

because a nanopyramid can directly absorb not only a portion of an incident wave but also the surrounding wave. It is well known that a small single particle can have a larger absorption cross section than its corresponding geometrical cross section [11, 32]. These results of confocal imaging indirectly prove that the nanopyramid arrays can realize ultra-high absorption in the visible regime.

4 Conclusions

In summary, a germanium nanopyramid array was proposed and fabricated. Both theoretical and experimental results verified that it is capable of achieving perfect absorption in the wavelength range from 500 to 800 nm; the absorption is as high as 100% in the characterization. We analyzed the phenomenon from the perspective of its physical mechanism by regarding germanium as a bulk material according to the corresponding band-gap theory. The high absorption coefficient of the nanopyramid arrays was investigated for application in light trapping, antireflection coating, and the slow-light mode. Considering the current high demand for the sustainable and green energy, it is reasonable to believe that the proposed absorber will find potential applications in areas related to light harvesting.

References

[1] Atwater, H. A.; Polman, A. Plasmonics for improved photovoltaic devices. *Nat. Mater*. **2010**, *9*, 205–213.

[2] Catchpole, K. R.; Polman, A. Plasmonic solar cells. *Opt. Express*. **2008**, *16*, 21793–21800.

[3] Zeng, B. B.; Gan, Q. Q.; Kafafi, Z. H.; Bartoli, F. J. Polymeric photovoltaics with various metallic plasmonic nanostructures. *J. Appl. Phys*. **2013**, *113*, 063109.

[4] Gan, Q. Q.; Bartoli, F. J.; Kafafi, Z. H. Plasmonic-enhanced organic photovoltaics: Breaking the 10% efficiency barrier. *Adv. Mater*. **2013**, *25*, 2385–2396.

[5] Gunawan, O.; Wang, K.; Fallahazad, B.; Zhang, Y.; Tutuc, E.; Guha, S. High performance wire-array silicon solar cells. *Prog. Photovoltaics*. **2011**, *19*, 307–312.

[6] Nelson, J. *Physics of Solar Cell*; Imperial College Press: London, 2008.

[7] Cao, L. Y.; Fan, P. Y.; Vasudev, A. P.; White, J. S.; Yu, Z. F.; Cai, W. S.; Schuller, J. A.; Fan, S. H.; Brongersma, M. L. Semiconductor nanowire optical antenna solar absorbers. *Nano Lett.* **2010**, *10*, 439–445.

[8] Guo, H. M.; Wen, L.; Li, X. H.; Zhao, Z. F.; Wang, Y. Q. Analysis of optical absorption in GaAs nanowire arrays. *Nanoscale Res. Lett.* **2011**, *6*, 617.

[9] Cao, L. Y.; White, J. S.; Park, J. S.; Schuller, J. A.; Clemens, B. M.; Brongersma, M. L. Engineering light absorption in semiconductor nanowire devices. *Nat. Mater.* **2009**, *8*, 643–647.

[10] Hu, L.; Chen, G. Analysis of optical absorption in silicon nanowire arrays for photovoltaic applications. *Nano Lett.* **2007**, *7*, 3249–3252.

[11] Tsai, S. J.; Ballarotto, M.; Romero, D. B.; Herman, W. N.; Kan, H. C.; Phaneuf, R. J. Effect of gold nanopillar arrays on the absorption spectrum of a bulk heterojunction organic solar cell. *Opt. Express.* **2010**, *18*, A528–A535.

[12] Fan, Z. Y.; Kapadia, R.; Leu, P. W.; Zhang, X. B.; Chueh, Y. L.; Takei, K.; Yu, K.; Jamshidi, A.; Rathore, A. A.; Ruebusch, D. J. et al. Ordered arrays of dual-diameter nanopillars for maximized optical absorption. *Nano Lett.* **2010**, *10*, 3823–3827.

[13] Fan, Z.; Razavi, H.; Do, J. W.; Moriwaki, A.; Ergen, O.; Chueh, Y. L.; Leu, P. W.; Ho, J. C.; Takahashi, T.; Reichertz, L. A. et al. Three-dimensional nanopillar-array photovoltaics on low-cost and flexible substrates. *Nat. Mater.* **2009**, *8*, 648–653.

[14] Wang, B. M.; Leu, P. W. Enhanced absorption in silicon nanocone arrays for photovoltaics. *Nanotechnology*. **2012**, *23*, 194003.

[15] Wang, K. X. Z.; Yu, Z. F.; Liu, V.; Cui, Y.; Fan S. H. Absorption enhancement in ultrathin crystalline silicon solar cells with antireflection and light-trapping nanocone gratings. *Nano Lett.* **2012**, *12*, 1616−1619.

[16] Zhu, J.; Yu, Z. F.; Burkhard, G. F.; Hsu, C. M.; Connor, S. T.; Xu, Y. Q.; Wang, Q.; McGehee, M.; Fan, S. H.; Cui, Y. Optical absorption enhancement in amorphous silicon nanowire and nanocone arrays. *Nano Lett.* **2009**, *9*, 279–282.

[17] Han, S. E.; Chen, G. Optical absorption enhancement in silicon nanohole arrays for solar photovoltaics. *Nano Lett.* **2010**, *10*, 1012–1015.

[18] Yahaya, N. A.; Yamada, N.; Kotaki, Y.; Nakayama, T. Characterization of light absorption in thin-film silicon with periodic nanohole arrays. *Opt. Express.* 2013, *21*, 5924–5930.

[19] Zhang, L. C.; Yang, G.; Wang, K.; Fu, M.; Wang, Y.; Long, H.; Lu, P. X. *Opt. Commun.* **2013**, *291*, 395–399.

[20] Lin, C. X.; Martínez, L. J.; Povinelli, M. L. Experimental broadband absorption enhancement in silicon nanohole structures with optimized complex unit cells. *Opt. Express*. **2013**, *21*, A872–A882.

[21] Liu, N.; Mesch, M.; Weiss, T.; Hentschel, M.; Giessen, H. Infrared perfect absorber and its application as plasmonic sensor. *Nano Lett*. **2010**, *10*, 2342–2348.

[22] Zhang, B. X.; Zhao, Y. H.; Hao, Q. Z.; Kiraly, B.; Khoo, I. C.; Chen, S. F.; Huang, T. J. Polarization-independent dual-band infrared perfect absorber based on a metal-dielectric-metal elliptical nanodisk array. *Opt. Express*. **2011**, *19*, 15221–15228.

[23] Hao, J. M.; Wang, J.; Liu, X. L.; Padilla, W. J.; Zhou, L.; Qiu, M. High performance optical absorber based on a plasmonic metamaterial. *Appl. Phys. Le*tt. **2010**, *96*, 251104.

[24] Liu, K.; Zeng, B. B.; Song, H. M.; Gan, Q. Q.; Bartoli, F. J.; Kafafi, Z. H. Super absorption of ultra-thin organic photovoltaic films. *Opt. Commun.* **2014**, *314*, 48–56.

[25] Ji, D. X.; Song, H. M.; Zeng, X.; Hu, H. F.; Liu, K.; Zhang, N.; Gan, Q. Q. Broadband absorption engineering of hyperbolic metafilm patterns. *Sci. Rep*. **2014**, *4*, 4498.

[26] Zeng, B. B.; Kafafi, Z. H.; Bartoli, F. J. Transparent electrodes based on two dimensional Ag nanogrids and double one-dimensional Ag nanogratings for organic photovoltaics. *J. Photon. Energy*. **2015**, *5*, 057005.

[27] Cui, Y. X.; Fung, K. H.; Xu, J.; Ma, H. J.; Jin, Y.; He, S. L.; Fang, N. X. Ultrabroadband light absorption by a sawtooth anisotropic metamaterial slab. *Nano Lett*. **2012**, *12*, 1443–1447.

[28] Fu, Y. Q.; Bryan, N. K. A.; San, O. A.; Hong, L. B. Data format transferring for FIB microfabrication. *Int. J. Adv. Manuf. Tech*. **2000**, *16*, 600–602.

[29] Fu, Y.; Bryan, N. K. A. Fabrication and characterization of slanted nanopillars arrays. *J. Vac. Sci. Technol. B*. **2005**, *23*, 984–989.

[30] Street, R. A. *Hydrogenated Amorphous Silicon*; Cambridge University Press: Cambridge, 1991.

[31] Shah, A. V.; Schade, H.; Vanecek, M.; Meier, J.; Vallat-Sauvain, E.; Wyrsch, N.; Kroll, U.; Droz, C.; Bailat, J. Thin-film silicon solar cell technology. *Prog. Photovoltaics*. **2004**, *12*, 113–142.

[32] Han, Q.; Jin, L.; Fu, Y. Q.; Yu, W. X. Polarization and incident angle insensitive germanium nano-pyramid array for perfect absorption in visible regime. *Insciences J*. **2014**, *4*, 19–26.

[33] He, J.; He, S. L. Slow propagation of electromagnetic waves in a dielectric slab waveguide with a left-handed material substrate. *IEEE Microw. Wirel. Co*. **2005**, *16*, 96–98.

[34] Jiang, T.; Zhao, J.; Feng, Y. Stopping light by an air waveguide with anisotropic metamaterial cladding. O*pt. Express*. **2009**, *17*, 170−177.

[35] Tsakmakidis, K. L.; Boardman, A. D.; Hess, O. 'Trapped rainbow' storage of light in metamaterials. *Nature*. **2007**, *450*, 397−401.